DOI 10.24425/aee.2023.146044

Controlling magnetic inductance by air-gap configuration in power electronics applications

RAFAL KASIKOWSKI

Institute of Electronics, Lodz University of Technology
93-590 Lodz, Poland
e-mail: *rafalkasikowski@p.lodz.pl*

(Received: 28.01.2023, revised: 13.03.2023)

Abstract: Gapped magnetic components are inherent to applications where conversion of power would force magnetic flux density beyond the saturation point of magnetic materials. A physical discontinuity in a magnetic path, which an air gap represents, signifies a drastic change in its reluctance to magnetic flux. This gives rise to a phenomenon referred to as the fringing effect, which impacts the performance of magnetic components. The fringing flux also affects the physical properties of magnetic components, such as magnetic reluctance and inductance. Since inductance of gapped magnetic components is a function of the size of the air gap, a relatively simple change to the configuration of the air gap or splitting a single gap into a plurality of gaps entails, frequently, a radical change to the magnetic circuit of the component. This paper examines the way the air-gap configuration affects the distribution of the fringing flux and, by extension, magnetic reluctance and inductance. A method to aid the design of multigap inductors is presented based on 3-D electromagnetic modelling as well as measurements. An analytic expression, which closely approximates the required length of quasi-distributed gaps substituting a single gap, is developed.

Key words: air gaps, electromagnetic modelling, magnetic cores, power electronics

1. Introduction

Magnetic components in energy storage and release applications are not able to store a significant amount of energy without the introduction of a physical discontinuity in their magnetic circuit in the form of an air gap. This relatively short path of high magnetic reluctance is integral in flyback transformers, ferrite inductors, power factor correction (PFC) chokes and, frequently, integrated LLC transformers (transformers in resonant converters where a resonant circuit consists of the primary and leakage inductance of the transformer and an external resonant capacitance),

to control the ratio of primary inductance to resonance inductance [1, 2]. Skilfully inserted gaps enhance the capability to handle substantial powers by a so-called shearing of the B-H loop, where the slope of the loop becomes flatter, and enable better control over changes in magnetic permeability μ due to temperature or excitation voltage [3]. As a consequence, higher electric currents, and, by extension, magnetic flux densities can be withstood by a given magnetic material. The incorporation of an air gap in a magnetic core impacts magnetic flux distribution along the magnetic path, and provokes magnetic field lines at the air gap to fringe out beyond the cross-sectional area of the core, [4–7] as illustrated in Fig. 1 in a schematized form and as magnetic field density distribution. This is referred to as the fringing effect phenomenon which may adversely impact the performance of magnetic components and alter their physical properties, namely magnetic reluctance and inductance. The fringing effect itself is rather complex, and, as a function of many variables, in particular the size of the air gap and the geometry of the core, as well as the shape and proximity of windings, eludes simple definition and measurement. One of the identifiable consequences of the fringing flux at an air gap is a reduction in the overall reluctance of the magnetic path, often referred to as a shortening of the gap. This is particularly evident for air gaps of comparatively large widths. In consequence, windings wound on cores featuring a single air gap exhibit higher inductance than that determined without taking the fringing magnetic flux into consideration. The discrepancy between the actual and the expected value of inductance yielded by basic computations is frequently represented by the so-called fringing-effect factor F – a ratio of the measured inductance to the inductance predicted but not accounting for the fringing effect [8]. Another consequence of the fringing magnetic flux at the air gap is embodied by electromagnetic interactions with the winding enclosing the gap. The induced eddy currents in the windings bring about extra power loss that manifests itself in the form of hot spots, as shown in Fig. 2.

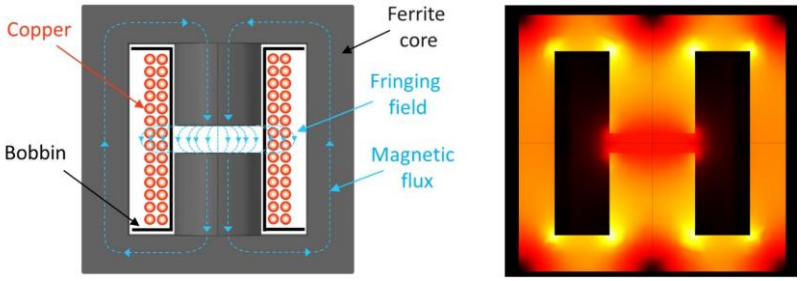

Fig. 1. Fringing magnetic field at air gap: left, schematized representation of phenomenon, right, modelling of magnetic field density distribution (thermal scale – COMSOL® 5.2a)

One of the simplest techniques for the reduction of the excess power loss associated with the fringing field is to prevent the stray magnetic flux from entering the windings by spacing the windings away from the gap or using electromagnetic interference (EMI) shielding in its immediate vicinity [9, 10]. Design engineers, due to the need for better thermal performance, frequently opt for multi-stranded, twisted wires or wires constructed according to a carefully arranged pattern known as litz wire [11]. In spite of their moderate simplicity, the techniques do not appear to offer the most effective solution, as they do not combat the origins of the problem,

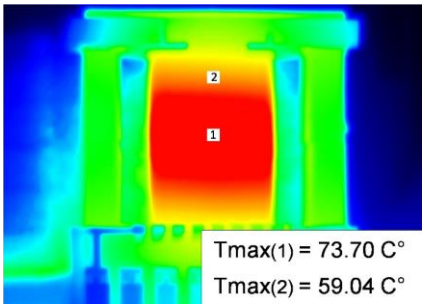

Fig. 2. Thermal image of inductor with single air gap

but only enable designing around it, and may reduce the available winding window, indirectly leading to elevated dissipation due to advantageous conditions for other power-loss mechanisms. Therefore, the quasi-distributed-gap technique, if properly implemented, appear, to offer the most effective method of reducing fringing-magnetic-flux power loss [12, 13].

As the fringing effect is a strong function of the length of the air gap, splitting a discrete gap into a number of gaps drastically affects the way the magnetic flux crosses the gaps, limiting the extent of its impact on the winding and the value of inductance. The fringing field phenomenon, in this case, seems to be largely confined to the immediate vicinity of the air gaps [14], Fig. 3. Intuitive reasoning would suggest that the splitting would be of no consequence to the physical properties of the component as long as the total length of discontinuity in the core remained unchanged. Indeed, an analogous conclusion can be drawn if we consider the expression commonly present in literature for inductance of a gapped core, Eq. (1), where the length of the gap can be given either as a single figure for the single gap or as a sum of the individual gaps. This would hold true if not for the fringing effect. In fact, Eq. (1) does not yield a correct value for the components' inductance for any air-gap configuration, as it does not take the fringing-magnetic-field phenomenon into consideration. Figure 4 illustrates two inductors with an identical total width of the air gaps, but with different air-gap configurations. Although the inductors were built on the same ferromagnetic cores, the coils consist of an identical number of turns, their inductance differs considerably, with

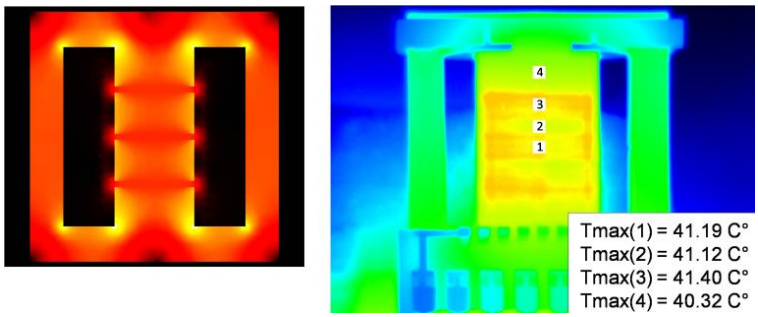

Fig. 3. Left, magnetic field density distribution in inductor with multi-gapped core (thermal scale – COMSOL® 5.2a); right, thermal image of inductor with quasi-distributed air gap

the dual-gap component having a value of inductance substantially lower than the single-gap inductor.

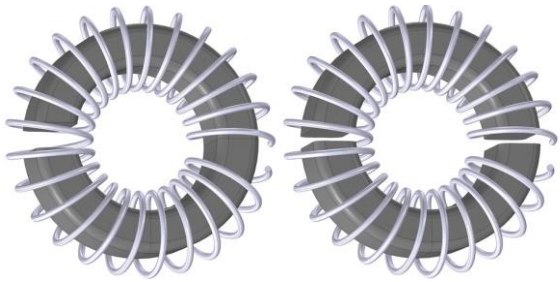

Fig. 4. Single-gap and dual-gap inductors of the same total air-gap length, core material and number of turns yielding different values of inductance

The mechanisms by which the stray magnetic flux at the vicinity of the air gaps and the positioning of discontinuities in the magnetic circuits influence local resistance to magnetic flux are, as yet, not fully explained [15]. For that reason, the problem of implementing the quasi-distributed gap into the component while maintaining the same inductance as its single-gapped counterpart, is not only a question of the size of the air gap.

It transpires that spaces between individual gaps and their placement along the core's column may, in a clearly measurable manner, impact the value of the inductance, Fig. 5.

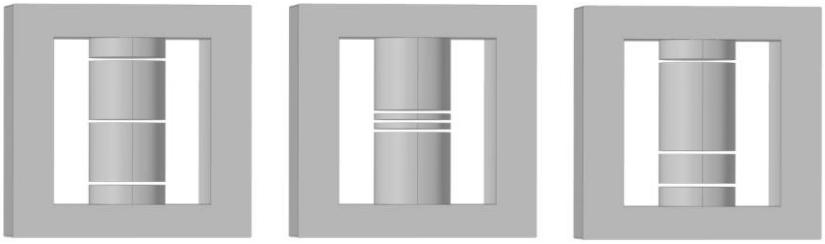

Fig. 5. Magnetic cores of the same material and total air-gap length, yielding different values of inductance for identical coils

There is a somewhat limited number of publications on the design of a quasi-distributed gap [16]. Even fewer papers touch the issue of splitting a single air gap into a number of individual gaps with the constraint of maintaining the same inductance of the component and hence the same operating conditions.

This concern appears relatively regularly in the design of magnetic components for Switch Mode Power Supplies (SMPS). A satisfactory solution to the said problem can be arrived at by trial and error, but this is an ineffective and time-consuming methodology in practical design. As there is no well-established method to implement a quasi-distributed gap that would produce the same inductance as the discrete gap, it appears logical to undertake the task of procuring a convenient technique for power supply designers. It is possible to run FEM (Finite Element

Method) simulations and tweak the lengths of individual gaps to give the wanted result, but this approach is not necessarily any more efficient than the trial-and-error method already mentioned. Preferably, the designers should be able to estimate the dimensions for a quasi-distributed gap without having to resort to time-consuming finite-element analysis.

2. Single-gap configuration

Magnetic reluctance, and hence, by extension, inductance, is a key characteristic of magnetic components. The commonly used expression for inductance of a gapped core (Eq. (1)) does not take the fringing effect into consideration and produces approximate results, or misleading results if air gaps of a substantial width are being considered.

$$L = \frac{N^2 \cdot \mu_0 \cdot A_e}{l_g + \dfrac{MPL}{\mu_r}}, \tag{1}$$

where: N is the number of turns, μ_0 is the permeability of free space, $4 \cdot \pi \cdot 10^{-7}$ H/m, A_e is the core cross sectional area, MPL is the magnetic path length, l_g is the air-gap length, μ_r is the relative permeability.

The utilization of Eq. (1) may bring satisfactory answers only if the impact of the fringing-flux phenomenon is taken into account and the equation is rewritten in a form which includes the fringing flux factor F Eq. (2):

$$L = F \cdot \left(\frac{N^2 \cdot \mu_0 \cdot A_e}{l_g + \dfrac{MPL}{\mu_r}} \right). \tag{2}$$

In general designation, Eq. (1) takes the following form, Eq. (3):

$$L = \frac{N^2}{R_C + R_G}, \tag{3}$$

where R_C is the reluctance of core material, Eq. (4).

$$R_C = \frac{MPL}{\mu_0 \cdot \mu_r \cdot A_e}. \tag{4}$$

R_G is the reluctance of an air gap, Eq. (5) (Fig. 6).

$$R_G = \frac{l_g}{\mu_0 \cdot A_G}. \tag{5}$$

A_G is the cross-sectional area of an air gap.

The expression for inductance of a gapped core in the form of Eq. (1) assumes that the cross-sectional area of both the core and the air gap are the same, $A_e = A_G$. This is in contrast to the fact that the magnetic field lines, while crossing the air gap, are no longer constrained by the core but fringe out into the neighbouring areas, thus extending the cross-sectional area of the air

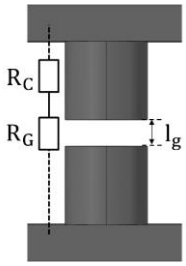

Fig. 6. Reluctance of magnetic core with single air gap

gap beyond the outline of the core. If we equate the two cross-sections, substituting Eq. (4) and Eq. (5) into Eq. (3) yields Eq. (1), the common expression for inductance of a gapped core.

Estimating an effective cross-sectional area of an air gap is rather complex, as many factors can contribute to the way in which the magnetic field lines are shaped in the vicinity of the gap. It appears the proximity of the windings, other sections of the core, as well as the positioning of the air gap along the core's column may affect the effective reluctance, and hence the resulting variations in the value of inductance. Figure 7 pictures ferrite cores of a different geometry, a RM12/I, E32/16/9 and an E42/21/15 type core [17], where, initially, their air gaps were positioned at the centre of the middle column carrying the winding, and then gradually shifted away from the centre. The value of the inductance tends to increase with the placement of the air gap being shifted away from the centre, up or down, with other parameters of the component kept unchanged. As a consequence, the value of inductance can be somewhat manipulated without a change in the size of the air gap.

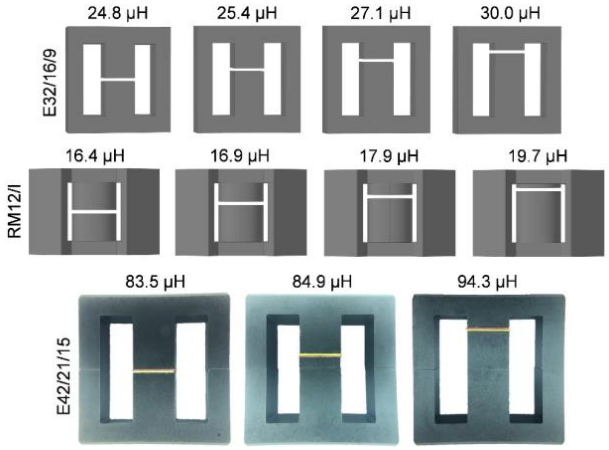

Fig. 7. E32/16/9 and RM12/I cores of the same material and air-gap width yielding different values of inductance for identical coils; practical verification using E42/21/15

A number of approaches have been developed to account for the impact of the fringing flux on primary magnetic properties, namely magnetic reluctance and inductance [18]. It is advocated in [8] to link the fringing-flux phenomenon to the geometry of a given core by the relation given

in Eq. (6). This approach seems to produce reliable values of inductance for the majority of single-gap cores of a relatively simple shape.

$$F = 1 + \frac{l_g}{\sqrt{A_e}} \cdot \ln\left(\frac{2 \cdot G}{l_g}\right), \tag{6}$$

where G is the core window length (winding width).

As shown herein, the fringing magnetic field at an air gap fringes out into the neighbouring areas, thus extending the cross-sectional area of the air gap beyond the outline of the core. Therefore the actual value of the reluctance of the air gap, and hence inductance of the component, can only be obtained if the cross-sectional area of the gap is somehow inflated. There are a number of views concerning the extent to which the spatial dimensions of the gap should increase [8, 18, 19]. One of the most elegant approaches is to represent the cross-sectional area as a function of the air-gap length l_g. Some research papers [20] postulate that the effective cross-sectional area of the gap that takes account of the fringing effect can be obtained by adding the air-gap length to each of the linear dimensions in the cross-section. This approach was explored herein for cores with distinct cross-sectional shapes: circular, square and rectangular, which were exemplified by the cores of ETD39//20/13, E32/16/9, and E42/21/15 types, respectively. Thus, for a round central column it is proposed to increase its radius r by l_g. This transforms the reluctance of a gap, Eq. (5), into the form of Eq. (7):

$$R_G = \frac{l_g}{\mu_0 \cdot \pi \cdot \left(r + l_g\right)^2}. \tag{7}$$

Now, the formula for inductance of the discussed single-gap inductor is as given in Eq. (8):

$$L = \frac{N^2}{\dfrac{MPL}{\mu_r \cdot \mu_0 \cdot A_e} + \dfrac{l_g}{\mu_0 \cdot \pi \cdot \left(r + l_g\right)^2}}. \tag{8}$$

Cores of a square cross-sectional area with the side length of a will, accordingly, have the reluctance of an air gap given as, Eq. (9):

$$R_G = \frac{l_g}{\mu_0 \cdot \left(a + l_g\right)^2}. \tag{9}$$

Hence, Eq. (10):

$$L = \frac{N^2}{\dfrac{MPL}{\mu_r \cdot \mu_0 \cdot A_e} + \dfrac{l_g}{\mu_0 \cdot \left(a + l_g\right)^2}}. \tag{10}$$

And, as follows, cores of rectangular cross-sectional areas $a \cdot b$ yield, Eq. (11) and Eq. (12):

$$R_G = \frac{l_g}{\mu_0 \cdot \left(a + l_g\right) \cdot \left(b + l_g\right)}, \tag{11}$$

$$L = \frac{N^2}{\dfrac{MPL}{\mu_r \cdot \mu_0 \cdot A_e} + \dfrac{l_g}{\mu_0 \cdot \left(a + l_g\right) \cdot \left(b + l_g\right)}}. \tag{12}$$

To verify the validity of this approach, numerical simulations with FEM were employed. The 3-D type model of a single-gap inductor with a copper coil mounted on the discussed cores was developed in the COMSOL®5.2a software environment. The computations were based on Maxwell's equations (Maxwell–Ampère's law and Gauss' law in the magnetic form) provided by the Magnetic Field interface in the AC/DC module of the program [21].

As solely magnetic inductance is to be computed, which, in essence, is a proportionality factor that depends on the geometry of a given magnetic component and its magnetic permeability, without modelling power loss, which is heavily frequency-dependent, the magnetostatic version of Maxwell's laws was utilized.

It has to be noted that in the case of ferrites, magnetic permeability is not frequency independent, and the measured values of inductance may somewhat differ from the modelled counterparts, especially for relatively high test frequencies.

A functional range of gap lengths typically appearing in SMPSs falls within 0.1 mm to 4 mm, where the latter should be considered relatively large. For that reason, the FEM simulations were run for that range with a fixed step of 0.1 mm. The gaps were positioned symmetrically in the middle of the central column carrying the winding. The winding itself was a single-layer copper coil of 1.32 mm diameter, wound on a phenolic bobbin, having 13 turns, 17 turns, and again 17 turns, for the E32/16/9, ETD39/20/13, and E42/21/15 cores, respectively. The cores were made of 3F3 ferrite material [22].

The results of the simulations run, the values of inductance yielded by the equation not taking account of the fringing flux (Eq. (1)), the values of inductance computed using the proposed equations (Eq. (8), Eq. (10), and Eq. (12)), and the values of inductance obtained by combining Eq. (2) and Eq. (6) are shown collectively in Fig. 8.

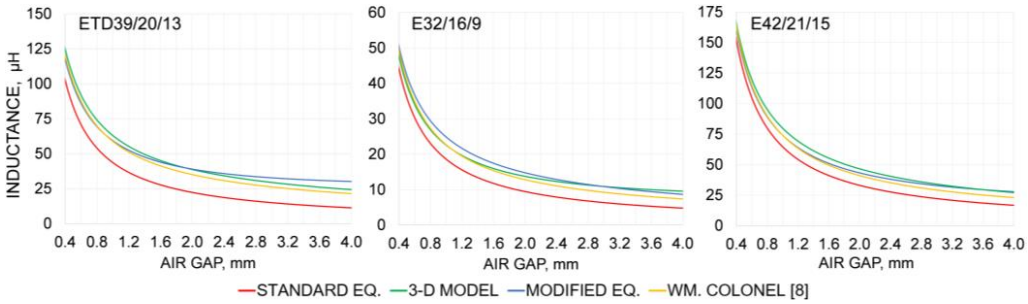

Fig. 8. Inductance values yielded by standard equation (red), 3-D model (green), modified equation (blue), and equation given in [8] for ETD, E32, and E42 type cores

The results yielded by the modified equations and the approach suggested in [8] remained largely consistent with the values of inductance computed in the modelling process for the considered air-gap range, whereas the traditional equation that does not reflect the impact of the fringing effect produced inductances significantly lower, especially for relatively large gaps. In the case of the ETD core the discrepancy between the model and the standard equation for a 4 mm gap was more than 50% (see Table 1).

Table 1. Relative error with respect to 3-D FEM models

	ETD39/20/13			**E42/21/15**			**E32/16/9**		
Gap mm	Standard equation	Modified equation	W. Colonel [8]	Standard equation	Modified equation	W. Colonel [8]	Standard equation	Modified equation	W. Colonel [8]
0.2	10.97%	4.02%	2.26%	2.88%	0.50%	1.11%	5.09%	1.63%	0.90%
0.4	17.73%	5.74%	3.64%	8.11%	3.16%	1.50%	12.10%	5.15%	2.46%
0.6	22.95%	6.42%	4.81%	12.43%	5.06%	3.77%	17.45%	7.30%	5.07%
0.8	27.19%	6.44%	5.81%	15.97%	6.31%	5.60%	21.68%	8.55%	7.09%
1	30.71%	5.94%	6.64%	19.01%	7.17%	7.19%	25.19%	9.23%	8.76%
1.2	33.75%	5.15%	7.41%	21.62%	7.69%	8.53%	28.08%	9.39%	10.05%
1.4	36.32%	3.99%	8.01%	23.84%	7.86%	9.61%	30.50%	9.14%	11.07%
1.6	38.61%	2.63%	8.56%	25.79%	7.80%	10.53%	32.58%	8.60%	11.89%
1.8	40.62%	1.07%	9.04%	27.52%	7.57%	11.33%	34.41%	7.86%	12.60%
2	42.43%	0.64%	9.48%	29.07%	7.17%	12.01%	36.01%	6.90%	13.16%
2.2	44.06%	2.49%	9.87%	30.45%	6.63%	12.60%	37.42%	5.76%	13.62%
2.4	45.53%	4.47%	10.22%	31.71%	5.98%	13.11%	38.67%	4.46%	13.98%
2.6	46.85%	6.61%	10.50%	32.85%	5.22%	13.56%	39.77%	3.00%	14.25%
2.8	48.08%	8.81%	10.79%	33.87%	4.34%	13.92%	40.76%	1.43%	14.47%
3	49.23%	11.07%	11.08%	34.81%	3.39%	14.25%	41.66%	0.25%	14.64%
3.2	50.27%	13.44%	11.33%	35.67%	2.34%	14.51%	42.45%	2.08%	14.72%
3.4	51.24%	15.92%	11.54%	36.45%	1.22%	14.73%	43.16%	4.02%	14.75%
3.6	52.13%	18.46%	11.74%	37.17%	0.03%	14.91%	43.83%	6.01%	14.79%
3.8	52.96%	21.10%	11.91%	37.82%	1.25%	15.05%	44.42%	8.12%	14.76%
4	53.73%	23.82%	12.07%	38.42%	2.59%	15.15%	44.94%	10.34%	14.69%

3. Quasi-distributed gap configuration

Evidence can be found that merely transforming a single air gap into a dual entity may bring about a significant alteration of the fringing flux distribution and result in a reduction in the discrepancy in temperature between the section of the winding located directly over the air gap and away from it [23]. If this were to be expanded to include a higher number of gaps in the magnetic path formed by consecutive subdivisions of the initial air gap, a further decrease in the effects of the fringing magnetic field would be observed. To demonstrate the above, the 3-D models of the cores shown in Section 2, were initially centre-gapped to 3 mm and then, gradually, the gap was successively partitioned with the constraint that the cumulative width of the gaps equals 3.0 mm. This led to a gradual reduction of the fringing-flux factor, and, as a consequence, the component's

inductance declined with the increasing number of gaps. Splitting the gaps into smaller entities continued until the cores featured 31 gaps (see Fig. 9), at which point the computed inductance was converging towards the values for the single-gap inductors yielded by Eq. (1) (14.94 µH, 6.32 µH, 22.14 µH for ETD39/20/13, E32/16/9, and E42/21/15, respectively), which did not take the fringing effect into consideration. In view of the above, it should be concluded that the final multi-gap configurations of the cores were no longer exhibiting any substantial increase in the inductance of the component, and hence the fringing magnetic field at the gap had been contained, essentially, within the cross-sectional area of the core. In the ideal scenario, where the fringing effect appears to be almost completely diminished, the fringing-flux factor would tend to 1.

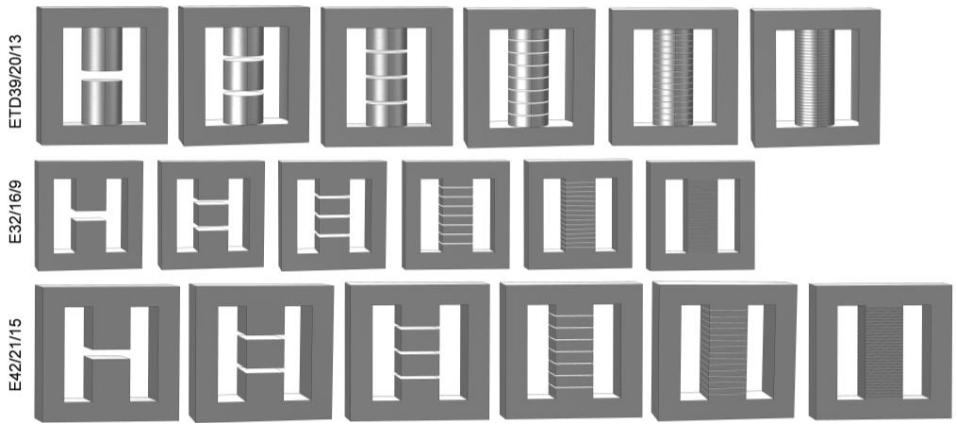

Fig. 9. Modelled cores configurations: single gap, double gap, three gaps, seven gaps, fifteen gaps and thirty-one gaps, all with total length of 3.0 mm. Top) ETD39/20/13, middle) E32/16/9, bottom) E42/21/15

Table 2 shows the collective results of the change in the fringing-flux factor as a function of the number of gaps. The FEM simulations proved that the fringing-effect factor, and thus the fringing-effect phenomenon itself, is a strong function of the size of the air gap, and with consecutive divisions of a discrete gap into an ever-increasing number of individual gaps of the same total length, the fringing flux factor F appears to tend towards 1.

Table 2. Fringing-flux factor and inductance for increasing number of gaps of the same total length

Number of gaps	Total gap length	The fringing-flux factor F			Inductance, µH		
		ETD39	E32	E42	ETD39	E32	E42
1	3.0 mm	1.736	1.714	1.534	25.918	10.840	33.975
2	3.0 mm	1.408	1.388	1.270	21.019	8.776	28.128
3	3.0 mm	1.297	1.280	1.183	19.372	8.093	26.195
7	3.0 mm	1.178	1.160	1.088	17.595	7.336	24.090
15	3.0 mm	1.134	1.114	1.051	16.932	7.048	23.280
31	3.0 mm	1.115	1.095	1.036	16.650	6.926	22.948

Since the presented pattern is only one of many possible designs of a quasi-distributed gap, it begs the question of to what extent an asymmetrical distribution would impact the value of the inductance. Given the dependency of this parameter on the fringing effect, and its increasing value for the stronger fringing magnetic fields, identifying the ideal distribution of individual gaps in a multiple-gap design would facilitate the optimization of a given magnetic component for the fringing-effect phenomenon. With this purpose, 3-D type FEM models of the single-coil inductors introduced in Section 2 of this paper were developed. As illustrated in Fig. 2 and Fig. 3, for the practical range of gap lengths used in SMPSs, splitting a single gap into just three individual gaps leads to a substantial reduction in the fringing effect. Incorporating a high number of gaps would cause extra power loss in core material, as shown in [24], and impact manufacturability. For that reason, the air gaps were restricted to three and five individual gaps, and the modelled cores featured these specific air-gap configurations. As the said cores come in pairs, which is also true for the majority of core types, it seemed to be a logical approach to position the central gap in the middle of the column. The outer gaps were to be initially adjacent to the gap, thereby forming a single gap, and then gradually moved away from the centre so that the resulting inductance L was a function of the distance between the gaps d_p (a so-called gap pitch). The length of each of the gaps l_g was fixed at 1.0 mm for the three-gap arrangement and at 0.6 mm for the five-gap arrangement, as uniform gap lengths ensure that no gap generates a stronger fringing magnetic field than the other. This is optimal from the point of view of the minimization of the fringing effect. It is no surprise that the biggest value of inductance L was found for the starting arrangements of the gaps, where the distance d_p between the gaps was equal to 0.0 mm, effectively forming a single, 3.0-mm air gap in the middle of the column. As the gap pitch gets larger, the inductance of the components gradually decreases, eventually reaching its minimum at about the point where the gaps, both in the three-gap and the five-gap arrangements, are exhibiting virtually a homogenous distribution over the entire length of the column (see Fig. 10). It becomes apparent that the impact of the fringing magnetic field on the total reluctance of the core, and thus the fringing factor F, is the weakest for this specific arrangement of the air gaps, and the higher the number of gaps, the stronger the reduction in the fringing magnetic flux.

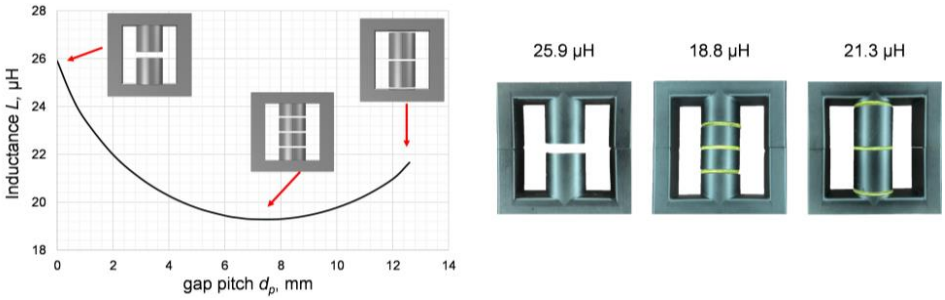

Fig. 10. Inductance L as function of gap pitch d_p for modelled 3F3 ETD39/20/13 inductor; practical verification using the same core

As the outer gaps were progressively moving away from the point of the lowest fringing-flux factor, the value of inductance was observed to gradually increase. However, by the time the gaps

neared the ends of the column, only a fraction of the maximum value registered for the single gap was regained. This appears to be valid for all the examined core types (Fig. 11).

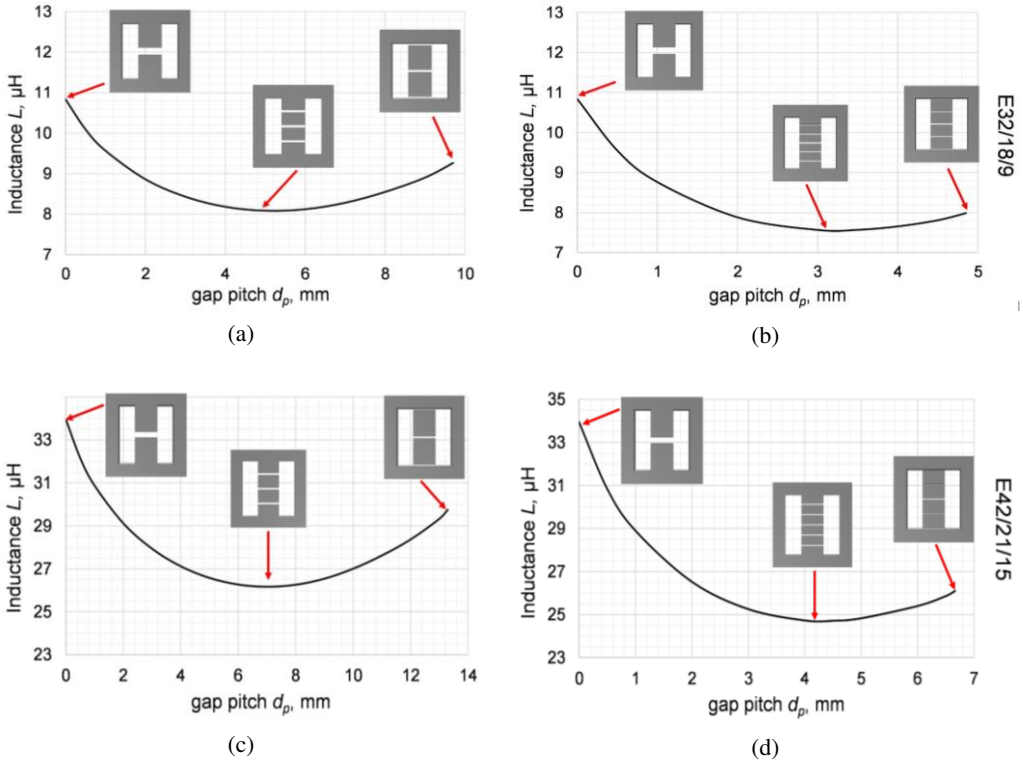

Fig. 11. Inductance L as function of gap pitch d_p for modelled inductors: 3-gap E32/16/9 (a); 5-gap E32/16/9 (b); 3-gap E42/21/15 (c); 5-gap E42/21/15 (d)

4. Constraint of maintaining the same inductance

The quasi-distributed-gap technique offers a very effective solution to combat some of the effects of the fringing flux, including the most adverse in the form of extra power dissipation. Despite the many upsides of this approach, the issue of splitting a single air gap into a number of individual gaps with the constraint of maintaining the same inductance of the component and hence the same operating conditions remains largely unresolved. This concern is, potentially, of considerable importance in many power electronics applications. Preferably, power supply designers should be able to arrive at the dimensions for a quasi-distributed gap without having to resort to complex numerical analysis. With the intention of establishing an analytical expression that would accelerate and aid the design process of quasi-distributed-gap magnetic components, a 3-D type FEM model of the inductors presented in the previous sections was utilized once more. The question of the choice of the gap pitch has been already resolved, as the impact of the

fringing effect on inductance is the weakest at the distance between gaps corresponding to their uniform distribution along the column carrying the coil (Fig. 11). Having established the pitch for each of the investigated core types, the length of the gap was set as a variable in the subsequently run simulations. The FEM simulations were executed, as previously, for the practical range of air gaps implemented in SMPSs with a fixed step of 0.1 mm. Initially, the value of inductance was computed for all single air gaps falling within the range, and subsequently, each of the single gaps was split into three, five and seven individual gaps of equal lengths. The length of individual gaps, for each of the cases, was finely tuned, with the constraint that the resulting inductance was the same for all the three-gap, five-gap, seven-gap models and the single-gap models corresponding to them. The results of the FEM simulations are shown collectively in Fig. 12. The presented plot can be used to identify, for each of the single gaps, a required total quasi-distributed-gap length that would yield the same inductance. The above should be considered valid for any magnetic component constructed on the base of an ETD39/20/13, E32/16/9 and E42/21/15. Furthermore, it is believed that satisfactory results can be procured also for other cores of an analogous shape. As illustrated in Fig. 12, for gaps of relatively short length, within the range of 0.1 mm to 0.4 mm, the relation between the length of single and quasi-distributed gaps is nearly linear, whereas for larger gaps the curve angles gradually away from the centre. This increasing discrepancy for larger gaps demonstrates that the quasi-distributed-gap technique is particularly effective in coils heavily impacted by the fringing-effect phenomenon.

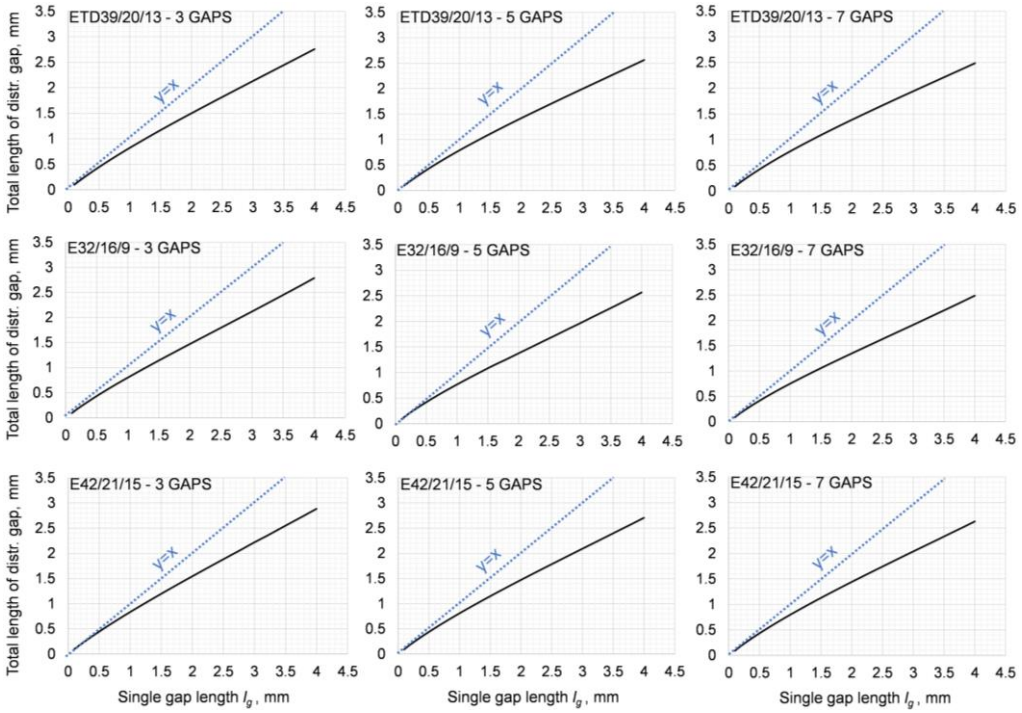

Fig. 12. Single-gap lengths and corresponding quasi-distributed-gap lengths that result in the same L if incorporated in magnetic components featuring ETD39/20/13, E32/16/9 and E42/21/15 type cores

To simplify the implementation of quasi-distributed gaps in the presented or analogous core types an empirical expression describing a quasi-distributed-gap length, as a function of the spatial dimensions of the core and the physical properties of a given magnetic component, is required. With this intention, Eq. (7)–(12) were modified to be applicable to cores with a plurality of gaps. For the quasi-distributed-gap configuration of Fig. 13 the equation describing magnetic reluctance and inductance for a round, square and rectangular central column take the following forms, Eq. (13)–(18):

For the round cross-sectional area:

$$R_G = \frac{n \cdot g}{\mu_0 \cdot \pi \cdot (r+g)^2}, \tag{13}$$

where g is the length of one of the gaps in the quasi-distributed air gap.

$$L = \frac{N^2}{\dfrac{MPL}{\mu_r \cdot \mu_0 \cdot A_e} + \dfrac{g}{\mu_0 \cdot \pi \cdot (r+g)^2}}. \tag{14}$$

For the square cross-sectional area:

$$R_G = \frac{n \cdot g}{\mu_0 \cdot (a+g)^2}, \tag{15}$$

$$L = \frac{N^2}{\dfrac{MPL}{\mu_r \cdot \mu_0 \cdot A_e} + \dfrac{n \cdot g}{\mu_0 \cdot (a+g)^2}}. \tag{16}$$

And for the rectangular cross-sectional area:

$$R_G = \frac{n \cdot g}{\mu_0 \cdot (a+g) \cdot (b+g)}, \tag{17}$$

$$L = \frac{N^2}{\dfrac{MPL}{\mu_r \cdot \mu_0 \cdot A_e} + \dfrac{n \cdot g}{\mu_0 \cdot (a+g) \cdot (b+g)}}, \tag{18}$$

where n is the number of individual air gaps.

The analytical expression necessary to calculate the dimensions of a quasi-distributed gap that would yield the same inductance as a single-gap component can be arrived at by solving Eq. (14),

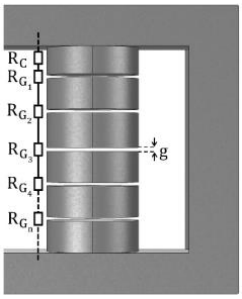

Fig. 13. Reluctance of magnetic core with quasi-distributed air gap

Eq. (16), and Eq. (18) for g. The other parameters are known, as they can be either found in the available literature or read from the manufacturer's data for the core and its material. As one can notice, the equations can be rewritten to the form of second-degree equations, and a series of mathematical transformations leads to the formulation of the following expressions:

For the round cross-sectional area, Eq. (19):

$$g = \frac{1 - 2 \cdot \beta \cdot r - \sqrt{1 - 4 \cdot \beta \cdot r}}{2 \cdot \beta}, \tag{19}$$

where

$$\beta = \frac{\left(N^2 - L \cdot R_C\right) \cdot \mu_0 \cdot \pi}{n \cdot L}. \tag{20}$$

For the square cross-sectional area, Eq. (21):

$$g = \frac{1 - 2 \cdot \beta \cdot a - \sqrt{1 - 4 \cdot \beta \cdot a}}{2 \cdot \beta}, \tag{21}$$

where

$$\beta = \frac{\left(N^2 - L \cdot R_C\right) \cdot \mu_0}{n \cdot L}. \tag{22}$$

And for the rectangular cross-sectional area, Eq. (23):

$$g = \frac{1 - \beta \cdot (a + b) - \sqrt{(\beta \cdot (a + b) - 1)^2 - 4 \cdot \beta^2 \cdot a \cdot b}}{2 \cdot \beta}, \tag{23}$$

where

$$\beta = \frac{\left(N^2 - L \cdot R_C\right) \cdot \mu_0}{n \cdot L}. \tag{24}$$

It has to be noted that the value of MPL in Eq. (4), if acquired from the core datasheet, shows MPL of an ungapped core, and, for that reason, it should be decreased by the length of the single gap l_g which is being replaced by the quasi-distributed gap. Hence, Eq. (25):

$$R_C = \frac{MPL - l_g}{\mu_0 \cdot \mu_r \cdot A_e}. \tag{25}$$

The procured analytical formulae (Eq. (19), Eq. (21) and Eq. (23)) were employed in the process of computing the size of the quasi-distributed gap for all corresponding single gaps from the modelled range of gaps and cores to see whether the results were compatible with the outcomes of the FEM simulations. The results yielded by the formulae and the 3-D models were put side by side and displayed collectively in Fig. 14 for an easy comparison.

One can see that the proposed expression approximates the simulations very closely for short and middle-size gaps, as both curves trail each other. For larger gaps, the results yielded by the expression deviate somewhat from the quasi-distributed-gap sizes predicted by the modelling, yet still appear to be quite accurate which is to be considered a satisfactory result.

As demonstrated, the conducted FEM simulations facilitated the task of constructing an approximate analytical formula that determines the size of the quasi-distributed gap replacing

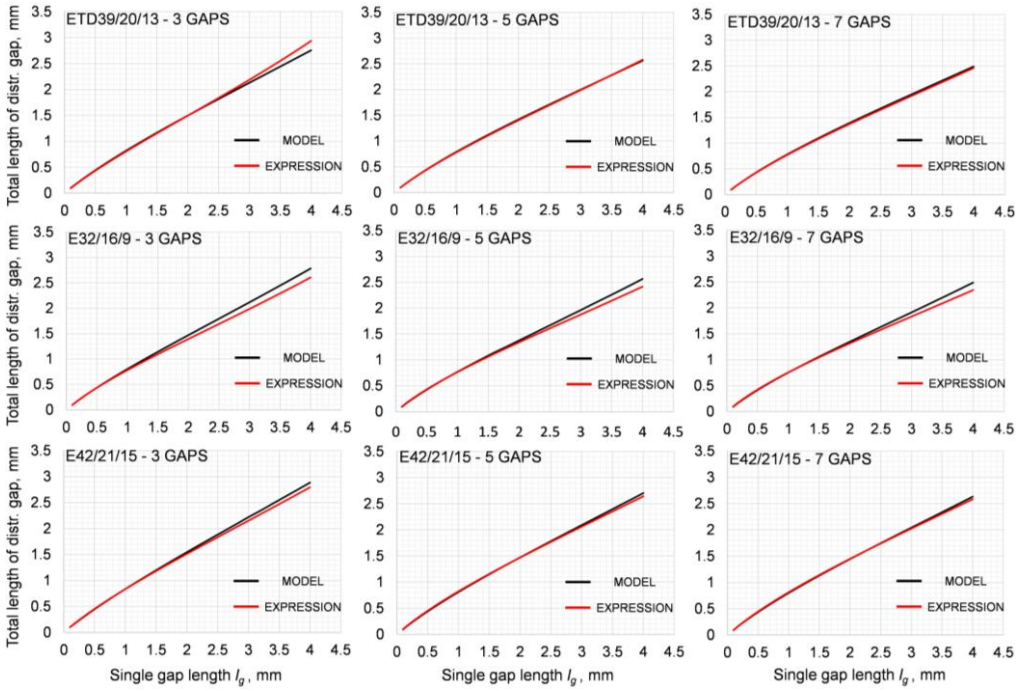

Fig. 14. Single-gap lengths and corresponding total quasi-distributed-gap lengths (red – formulae, black – FEM computations) that result in the same L if incorporated in magnetic components featuring ETD39/20/13, E32/16/9 and E42/21/15 type cores

a single discrete gap without a change in the inductance of the magnetic component. The composed expression is valid for magnetic components built on cores of the examined types. However, it is believed that an analogous technique can be extended to different core shapes by linking the length of the gap to the linear dimensions in the cross-section of the core.

The practical verification of the formulated expressions (Eq. (19), Eq. (21) and Eq. (23)) was firstly carried out for the E39/20/13 type inductor carrying a 17-turn coil. Initially, the core of the constructed inductor had a single gap of about 3.8 mm. Subsequently, the gap was split into three individual gaps with an effective length of about 2.7 mm, according to Eq. (19), to yield the same value of inductance as its single-gap counterpart (see Fig. 15). The measured inductance was

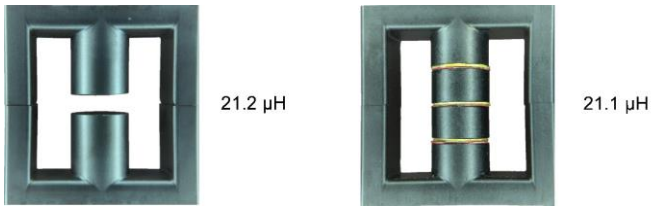

Fig. 15. Practical verification of developed analytical expressions using E39/20/13 type core

about 21.2 μH and 21.1 μH for the single-gap component and three-gap component, respectively. This, in principle, proves the validity of the procured analytical formulae.

A further experimental verification of the formulae was conducted for a E42/21/15 type core of a rectangular cross-sectional area. In this case, a single discreet gap of 3.17 mm was replaced with three individual gaps with an effective length of about 2.25 mm (according to Eq. (23)) to yield the same value of inductance as its single-gap counterpart (see Fig. 16). The constructed components had the same 17-turn winding resulting in the value of inductance of 31.6 μH for both.

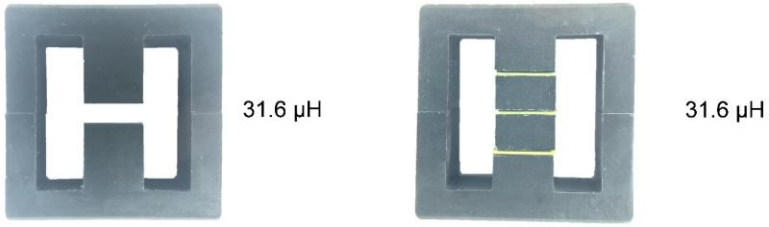

Fig. 16. Practical verification of developed analytical expressions using E42/21/15 type core

5. Conclusions

The FEM-based simulations and the constructed physical magnetic components examined herein visualised the impact of the fringing flux at the air gap on magnetic reluctance and inductance. The modelled inductors featuring ETD39/20/13, E32/16/9, E42/21/15 type cores, of a circular, square and rectangular cross-sectional area, showed the dependency of these properties on the positioning of a single air gap along the core's column. The fringing-flux factor F, as demonstrated, shows strong dependency on the size and the number of air gaps. The size of individual gaps in a distributed gap, if adequately selected, leads to significant reduction in the impact that the fringing magnetic field exerts on the value of inductance, thereby bringing the value of the fringing-flux factor down towards one.

As shown herein, the equation regularly used to calculate the value of inductance (Eq. (1)), and its modified version obtained by combining Eq. (2) and Eq. (6), do not yield correct results for magnetic components with an air gap for different configurations of the air gap. The former will not procure accurate values of inductance for any air-gap configurations, as it does not take the fringing-flux phenomenon into consideration, and the latter (Eq. (6)) is not applicable to multi-gap configurations.

The FEM representation of the inductors and the subsequently run simulations showed that the distance between the gaps in a multi-gap core can be optimized. It was shown that uniform distribution along the length of the core column is most favourable from the point of view of minimization of the fringing effect.

The issue of incorporating a quasi-distributed gap into a magnetic path of components without impacting their primary physical properties was also confronted. The series of FEM simulations were conducted in order to simplify the design of quasi-distributed gaps so that power supply

engineers no longer have to rely on hit-and-miss or other typically time-consuming methods. This led to the formulation of empirical expressions (Eq. (19), Eq. (21), and Eq. (23)) that can be fairly straightforwardly implemented in the process of designing magnetic components where a single discrete gap is substituted with multiple air gaps for cores with distinct cross-sectional shapes: circular, square and rectangular.

It has to be noted that the presented equations may produce inconsistent or somewhat different results for cores of distinct shapes to those investigated, where the middle column carrying the winding is very short in respect to the size of the core or for cores of custom shapes. Applicability of the procured formulae to cores with air-gap configurations consisting of a much higher number of individual gaps than those examined may be somewhat reduced. The presented air-gap configurations were chosen due to manufacturability and core-loss minimisation constraints. The degree of the utilization of the winding window area and tolerances in spatial dimensions of individual cores may also introduce certain discrepancies.

References

[1] Jung J.H., *Bifilar Winding of a Center-Tapped Transformer Including Integrated Resonant Inductance for LLC Resonant Converter*, IEEE Transactions on Power Electronics, vol. 28, no. 2, pp. 615–620 (2013), DOI: 10.1109/TPEL.2012.2213097.

[2] Moradewicz A.J., Kazmierkowski M.P., *High efficiency contactless energy transfer system with power electronic resonant converter*, Archives of Electrical Engineering, vol. 57, no. 4, pp. 375–381 (2009), DOI: 10.2478/v10175-010-0141-0.

[3] Kaiser K.L., *Magnetic Materials and a Few Devices*, in Electromagnetic Compatibility Handbook, 1st ed., CRC Press (2004).

[4] Yang R.S., Hanson A.J., Reese B.A., Sullivan C.R., Perreault D.J., *A low-loss inductor structure and design guidelines for high-frequency applications*, IEEE Transactions on Power Electronics, vol. 34, no. 10, pp. 9993–10005 (2019), DOI: 10.1109/TPEL.2019.2892397.

[5] Jez R., *Influence of the distributed air gap on the parameters of an industrial inductor*, IEEE Transactions on Magnetics, vol. 53, no. 11 (2017), DOI: 10.1109/TMAG.2017.2699120.

[6] Tian Y., Li Y., Liu J., *Fringing Field Analytical Calculation of High Frequency Planar Magnetic Components*, CPSS Transactions on Power Electronics and Applications, vol. 7, no. 3, pp. 251–258 (2022), DOI: 10.24295/CPSSTPEA.2022.00023.

[7] Keerthi Sudha B.V.K.S.L., Sirija R., Sravan Kumar V.S., *Analysis of Impact of Fringing on Design of Inductors with Air Gaps*, in 2022 IEEE 19th India Council International Conference (INDICON), Kochi, India (2022).

[8] Colonel W., McLyman T., *Fundamentals of Magnetics*, in *Transformer and Inductor Design Handbook, Design Handbook*, 4th ed., CRC Press (2011).

[9] Simpson N., Mellor P.H., *Additive manufacturing of shaped profile windings for minimal AC loss in gapped inductors*, in 2017 IEEE International Electric Machines and Drives Conference (IEMDC), Miami, FL, USA (2017).

[10] Pollock J.D., Sullivan C.R., *Gapped-inductor foil windings with low AC and DC resistance*, in Conf. Record of the 2004 IEEE Industry Applications Conference, Seattle, WA, USA (2004).

[11] Barlik R., Nowak M., Grzejszczak P., Zdanowski M., *Analytical description of power losses in a transformer operating in the dual active bridge converter*, Archives of Electrical Engineering, vol. 64, no. 3, pp. 561–574 (2016), DOI: 10.1515/bpasts-2016-0063.

[12] Wang C.-M., Seto K., Yoon S., Nomura T., *Planar inductor with quasi-distributed gap core and busbar based planar windings*, in 2013 IEEE Energy Conversion Congress and Exposition (ECCE), Denver, USA (2013).

[13] Hu J., Sullivan C.R., *AC resistance of planar power inductors and the quasi-distributed gap technique*, IEEE Transactions on Power Electronics, vol. 16, no. 4, pp. 558–567 (2001), DOI: 10.1109/63.931082.

[14] Kasikowski R., Więcek B., *Fringing-Effect Losses in Inductors by Thermal Modelling and Thermographic Measurements*, IEEE Transactions on Power Electronics, vol. 36, no. 9, pp. 9772–9786 (2021), DOI: 10.1109/TPEL.2021.3058961.

[15] Akbari M., Rezaei-Zare A., Cheema M.A.M., Kalicki T., *Air Gap Inductance Calculation for Transformer Transient Model*, IEEE Transactions on Power Delivery, vol. 36, no. 1, pp. 492–494 (2021), DOI: 10.1109/TEC.2020.3009818.

[16] Hao S., Zhang Z., Li J., Han J., *Analysis of Distributed Air Gap Parameters of Differential Mode Inductor Considering Core Loss and Saturation*, in 2019 22nd International Conference on Electric Machines and Systems (ICEMS), Harbin, China (2019).

[17] Ferroxcube Data Handbook, *Soft Ferrites and Accessories*, Ferroxcube, pp. 257, 270, 831 (2013).

[18] Balakrishnan A., Joines W.T., Wilson T.G., *Air-Gap Reluctance and Inductance Calculations for Magnetic Circuits Using a Schwarz–Christoffel Transformation*, IEEE Transactions on Power Electronics, vol. 12, no. 4, pp. 654–663 (1997), DOI: 10.1109/63.602560.

[19] Roshen W.A., *Fringing Field Formulas and Winding Loss Due to an Air Gap*, IEEE Transactions on Magnetics, vol. 43, no. 8, pp. 3387–3394 (2007), DOI: 10.1109/TMAG.2007.898908.

[20] Hurley W.G., Wölfle W.H., *Transformers and inductors for power electronics: theory, design and applications*, John Wiley and Sons Ltd. (2013).

[21] COMSOL, *COMSOL Multiphysics Reference Manual*, version: COMSOL 5.2a.

[22] Ferroxcube Data Handbook, *Soft Ferrites and Accessories*, Ferroxcube, pp. 123–124 (2013).

[23] Kasikowski R., Spriddell D., Howes G., *Evaluating Fringing Effects in Multi Gapped Toroids*, Bodo's Power Systems, pp. 22–24 (2018).

[24] Neumayr D., Bortis D., Kolar J.W., Hoffmann S., Hoene E., *Origin and quantification of increased core loss in MnZn ferrite plates of a multi-gap inductor*, CPSS Transactions on Power Electronics and Applications, vol. 4, no. 1, pp. 72–93 (2019), DOI: 10.24295/CPSSTPEA.2019.00008.